Modeling of the Divergently Worn Annular Seal for the Two-Way Coupled Fluid–Structure Interaction Analysis of Shaft Vibration and Clearance Flow

Shogo Kimura[1(✉)], Tsuyoshi Inoue[1], Hiroo Taura[2], and Akira Heya[1]

[1] Nagoya University, Aichi, Japan
kimura.shogo.f2@s.mail.nagoya-u.ac.jp,
inoue.tsuyoshi@nagoya-u.jp, akira.heya@mae.nagoya-u.ac.jp
[2] Kindai University, Osaka, Japan
taura@mech.kindai.ac.jp

Abstract. One of the causes of shaft vibration in turbomachinery is the rotordynamic (RD) fluid force. RD fluid force has a significant impact on the stability of the system, so it is necessary to carry out shaft vibration analysis considering the influence of RD fluid force at the design stage. The common methods for considering the effect of RD fluid force in shaft vibration analysis are linear RD coefficients and two-way coupled analysis. In the previous research, two-way coupled analysis was validated by experiment. However, Onset Speed of Instability (OSI) changed as experiment was repeated due to wear of seal stator. In order to explain this change, two-way coupled analysis of the clearance flow and shaft vibration of the divergent tapered annular seal was performed. In particular, the modeling of the clearance flow of the divergent tapered annular seal was investigated by detailed comparison with CFD analysis of the pre-swirl ratio and loss coefficient at the inlet. Two-way coupled analysis of the clearance flow and shaft vibration of the divergent tapered annular seal incorporating this model was conducted to determine the OSI. The results were compared with experimental results and discussed.

Keywords: FSI analysis · Divergent tapered seal · Shaft vibration · Clearance flow

1 Introduction

Rotordynamic (RD) fluid force generated at the seals is one of the causes contributing to shaft vibration in turbomachinery [1]. RD fluid force is generated by the interaction between shaft vibration and fluid and has a significant influence on the stability of the system, so shaft vibration analysis considering the influence of RD fluid force is necessary at the design stage.

There are two types of shaft vibration analyses which consider the influence of RD fluid force: the method using linear RD coefficients and Fluid-Structure Interaction (FSI)

F. Chu and Z. Qin (Eds.): IFToMM 2023, MMS 140, pp. 409–418, 2024.
https://doi.org/10.1007/978-3-031-40459-7_28

analysis. Bulk-Flow analysis [2] and CFD analysis [3] are two methods for obtaining linear RD coefficients. In these methods, the RD coefficient is obtained by linearising the RD fluid force around the centre of the seal or static eccentricity. However, the prediction of linear RD coefficients is based on the assumption that the whirling amplitude is small and cannot consider the non-linearity of the RD fluid force. On the other hand, FSI analysis is a method of shaft vibration analysis that can be applied when the whirling amplitude is large and the non-linearity of the RD fluid force is pronounced. Miyake et al. [4] and Kunori et al. [5] used this method to determine the Onset Speed of Instability (OSI) of a vertical shaft system supported by a plain annular seal and compared the OSI with experimental results. The frequency responses obtained from the experiments are shown in Fig. 1.

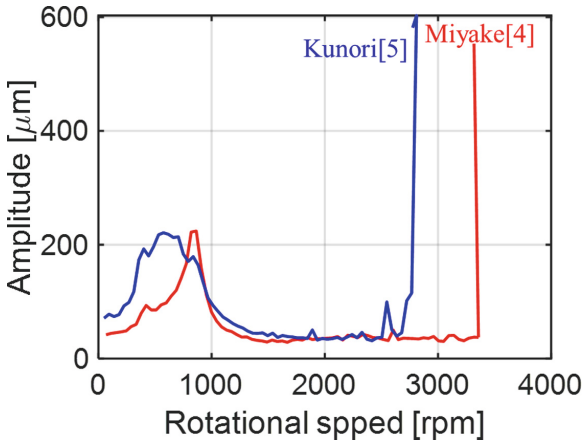

Fig. 1. Comparison of frequency responses obtained from experiments [4, 5]

Comparing the result of the experiment conducted by Miyake et al. [4] with one conducted by Kunori et al. [5], the OSI dropped from 3357 rpm to 2828 rpm as shown in Fig. 1, a difference of 529 rpm, even though the same experimental apparatus was used. This is thought to be due to the stator being worn as the experiment was repeated, as the rotor contacted the stator after the rotational speed exceeded the OSI in the experiment. The radial clearance was 200 μm when the seal was made, but as the experiment was repeated, the radial clearance increased due to wear, and it was found that the seal went from a plain annular seal to a divergent tapered annular seal. The measurement positions and the clearance are shown in Fig. 2.

Since it has been shown that the direct damping and direct stiffness coefficients among the RD coefficients are reduced in divergent tapered annular seal [6], resulting in reduced stability, the FSI analysis of a vertical shaft supported by a divergent tapered annular seal is carried out by expanding the conventional FSI analysis for a plain annular seal [4, 5]. The change in stator geometry due to the taper causes change in the flow at the seal inlet and outlet compared to the plain annular seal case, and the boundary conditions such as pre-swirl ratio and loss coefficients are considered to change. These coefficients have a significant influence on the dynamic characteristics of the seal and

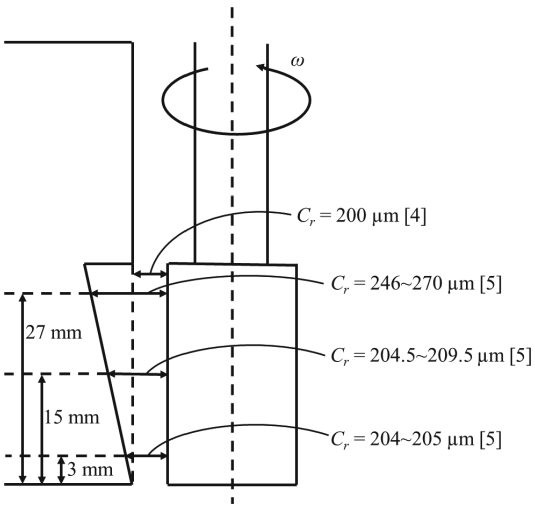

Fig. 2. Measurement position and seal clearance

need to be estimated accurately. The pre-swirl ratio and loss coefficient at the seal inlet are obtained by CFD analysis and applied as boundary conditions in the clearance flow analysis of the FSI analysis to accurately model the divergent tapered annular seal. The results are compared with experimental results.

2 CFD analysis for boundary condition parameter estimation

The analysis domain used in the CFD analysis is shown in Fig. 3. In addition to the seal section, a preliminary region is set at both the seal inlet and outlet sides as the analysis domain. The length of the preliminary region is 1/4 of the length of the seal section [7].

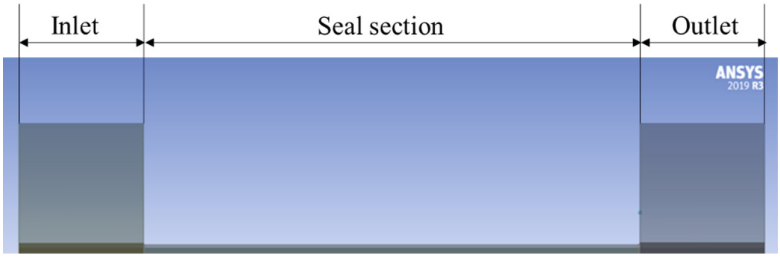

Fig. 3. Analysis domain of CFD analysis

2.1 Estimation of pre-swirl ratio

The average circumferential velocity inside the seal is calculated from the circumferential velocity distribution by CFD analysis and the circumferential velocity v_{in} at the seal inlet is calculated by extrapolation to obtain the pre-swirl ratio α using Eq. (1).

$$\alpha = \frac{v_{in}}{R\omega} \tag{1}$$

where R is the rotor radius and ω is the rotor rotational speed. The area-weighted average is used to calculate the average value of the circumferential velocity. If the total area of the meshes at the seal inlet is A, the area of each mesh is A_i and the circumferential flow velocity at each mesh is v_i, the circumferential flow velocity v_{in} at the seal inlet is expressed by Eq. (2) [8].

$$v_{in} = \frac{1}{A}\sum_i v_i A_i \tag{2}$$

2.2 Estimation of loss coefficient

From the axial velocity distribution, the average axial velocity inside the seal is determined and extrapolated to calculate the axial velocity at the seal inlet and outlet. The pressure at the seal inlet and outlet is calculated by extrapolation from the pressure distribution inside the seal. These are substituted into Eq. (3) (Bernoulli's equation) to calculate the loss coefficients at the inlet and outlet. The area-weighted average is used to calculate the average axial velocity.

$$\begin{aligned} P_s &= p_{in} + \frac{1}{2}\rho(1+\xi_s)w_{in}^2 \\ P_e &= p_{out} + \frac{1}{2}\rho(1-\xi_e)w_{out}^2 \end{aligned} \tag{3}$$

3 FSI analysis for divergent tapered annular seal

3.1 Rotor system model

As an analytical model, the two-disk vertical elastic shaft model used in the literature [4, 5] is used: two disks are mounted on a shaft, with simple support at the upper end and seal support at the lower end; the RD fluid force acts on the disk at the seal. The equation of motion for this rotor system is expressed by Eq. (4).

$$M\ddot{\mathbf{q}} + C\dot{\mathbf{q}} + \mathbf{K}\mathbf{q} = \mathbf{F}_{unb} + \mathbf{F}_{RD} \tag{4}$$

where $\mathbf{M}$ is mass matrix, $\mathbf{C}$ is damping matrix, $\mathbf{K}$ is stiffness matrix, $\mathbf{q}$ is displacement vector, $\mathbf{F}_{\mathrm{unb}}$ is the unbalance force and $\mathbf{F}_{\mathrm{RD}}$ is the RD fluid force.

3.2 Clearance flow analysis

While the previous research [4, 5] focused on plain annular seal, the present study extends the scope to divergent tapered annular seal. The clearance h between the rotor and stator in divergent tapered annular seal is expressed by Eq. (5).

$$h(\theta, z) = C_r - q_{sx}\cos\theta - q_{sy}\sin\theta + \varphi z \tag{5}$$

where C_r is the seal radial clearance, q_{sx} and q_{sy} are the rotor displacements, φ is the taper angle, θ is the circumferential coordinate and z is the axial coordinate. The governing equations for the clearance flow analysis are Eqs. (6), (7) and (8).

$$\rho\left\{\frac{\partial h}{\partial t} + \frac{\partial(hv)}{\partial y} + \frac{\partial(hw)}{\partial z}\right\} = 0 \tag{6}$$

$$\rho\left\{\frac{\partial(hv)}{\partial t} + \frac{\partial\left(hv^2\right)}{\partial y} + \frac{\partial(hwv)}{\partial z}\right\} + h\frac{\partial p}{\partial y} + \tau_{ry} + \tau_{sy} = 0 \tag{7}$$

$$\rho\left\{\frac{\partial(hw)}{\partial t} + \frac{\partial(hvw)}{\partial y} + \frac{\partial\left(hw^2\right)}{\partial z}\right\} + h\frac{\partial p}{\partial z} + \tau_{rz} + \tau_{sz} = 0 \tag{8}$$

where $y\ (= R\theta)$ is the circumferential coordinate, v is the circumferential flow velocity, w is the axial flow velocity, p is pressure, ρ is density of fluid and τ is sheer stress. The pressure distribution in the seal is obtained by solving Eq. (9) derived from these governing equations.

$$\begin{aligned}-(\nabla h\cdot\nabla p + h\nabla^2 p) = \rho\Bigg[\frac{\partial}{\partial t}\left\{\frac{\partial(hv)}{\partial y} + \frac{\partial(hw)}{\partial z} + \frac{\partial h}{\partial t}\right\} - \frac{\partial^2 h}{\partial t^2} + \frac{\partial^2(hv^2)}{\partial y^2} + 2\frac{\partial^2(hvw)}{\partial y\partial z} \\ + \frac{\partial^2(hw^2)}{\partial z^2}\Bigg] + \frac{\partial}{\partial y}(\tau_{sy} + \tau_{ry}) + \frac{\partial}{\partial z}(\tau_{sz} + \tau_{rz})\end{aligned} \tag{9}$$

Equation (3) is used as a boundary condition when solving the Eq. (9). The obtained pressure is integrated over the rotor surface as shown in Eq. (10) to obtain the RD fluid force $\mathbf{F}_{\mathrm{RD}}$ acting on the rotor.

$$\begin{cases} F_{RDx} = -\iint p\cos\theta d\theta dz \\ F_{RDy} = -\iint p\sin\theta d\theta dz \end{cases} \tag{10}$$

4 Results and discussion

4.1 Pre-swirl Ratio

Figure 4(a) shows the distribution of circumferential flow velocities in all meshes of the plain annular seal. The average value of the circumferential velocity is shown as the red circle in Fig. 4(b). The circumferential flow velocity v_{in} at the seal inlet was obtained by extrapolation from the average value of the circumferential flow velocity inside the seal.

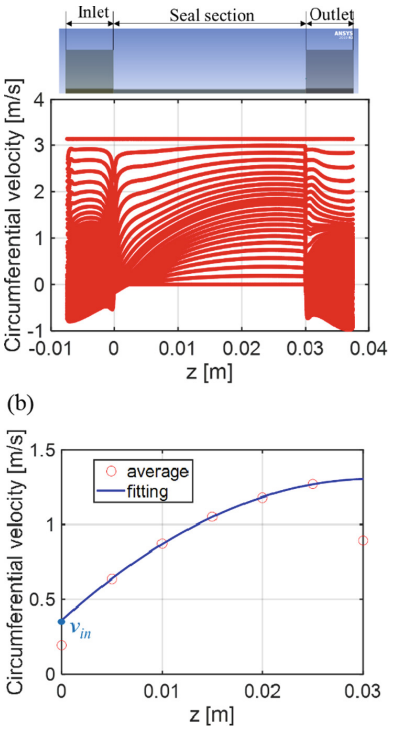

Fig. 4. Circumferential velocity distribution in all meshes (a) and average circumferential velocity (red circle) and approximating curve (blue line) (b) (Color figure online)

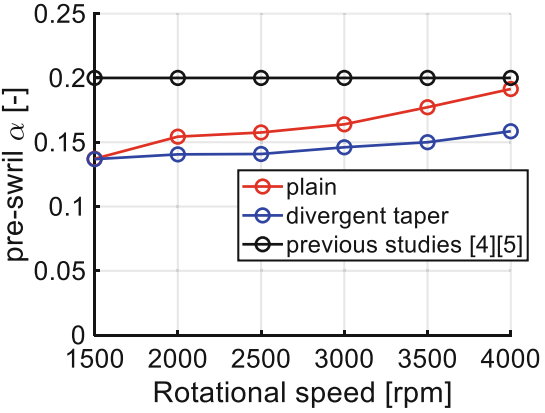

Fig. 5. Comparison of pre-swirl ratio in plain annular seal, divergent tapered annular seal and previous studies [4, 5]

The pre-swirl ratio obtained for the plain annular seal and the divergent tapered annular seal are shown in Fig. 5.

In previous studies [4, 5], the pre-swirl ratio for plain annular seal was assumed to be constant at 0.2 irrespective of the rotational speed, as shown by the black line. The pre-swirl ratio increases with increasing rotational speed for both plain annular seal and divergent tapered annular seal. The pre-swirl ratio for the plain annular seal is higher than that for divergent tapered annular seal. This can be attributed to the fact that the circumferential shear force is reduced due to the increased average clearance caused by the taper, which also reduces the circumferential flow velocity.

4.2 Inlet Loss Coefficient

The pressure and axial velocity distributions were calculated for the plain annular seal and the divergent tapered annular seal, respectively, and the axial velocity and pressure at the seal inlet and outlet were determined as shown in Figs. 6 and 7.

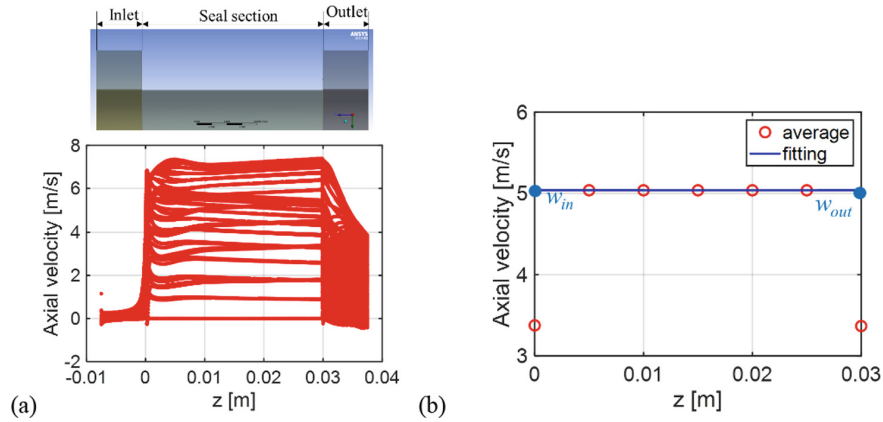

Fig. 6. Axial velocity distribution in all meshes (a) and average axial velocity (red circle) and approximating line (blue line) (b) (Color figure online)

The inlet loss coefficients obtained for the plain annular seal and the divergent tapered annular seal are shown in Fig. 8.

In previous studies [4, 5], the inlet loss coefficient for plain annular seal was assumed to be constant at 0.5 irrespective of the rotational speed, as shown by the black line. For plain annular seal, the inlet loss coefficient increases with increasing rotational speed. On the other hand, the value is almost constant for the divergent tapered annular seal, irrespective of the rotational speed. The inlet loss coefficient for the divergent tapered annular seal is higher. This is due to the fact that, as shown in Fig. 9, the vortex is generated over a wider area at the inlet of the divergent tapered annular seal due to the longer distance between the flow separation and reattachment to the stator wall.

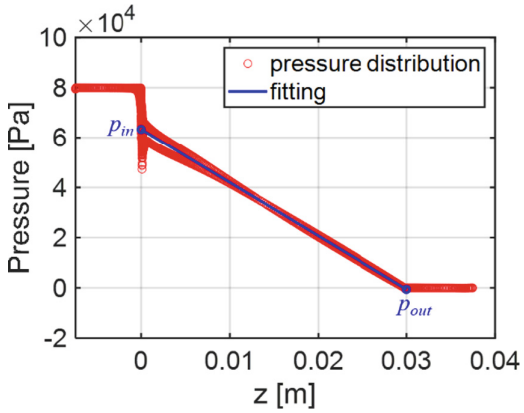

Fig. 7. Pressure distribution in all meshes (red circle) and approximation line of pressure inside of the seal (blue line) (Color figure online)

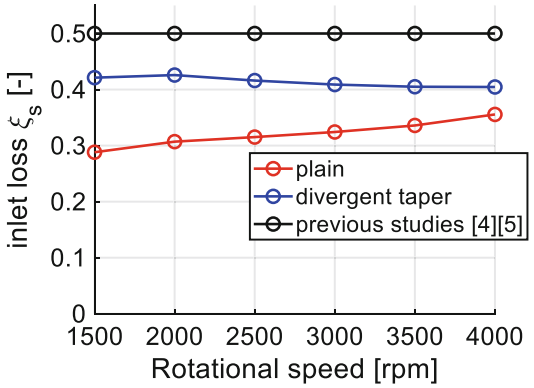

Fig. 8. Comparison of inlet loss coefficient in plain annular seal, divergent tapered annular seal and previous studies [4, 5]

4.3 Onset Speed of Instability

In the case of the divergent tapered annular seal, the pre-swirl ratio and inlet loss coefficient obtained from the CFD analysis were used in the FSI analysis to obtain the OSI. The RD coefficients were derived using the pre-swirl ratio and inlet loss coefficients obtained from the CFD analysis and the OSI was obtained by eigenvalue analysis. The OSI obtained from the FSI and eigenvalue analysis and the OSI obtained from the experiments [4, 5] are shown in Fig. 10, for the same pre-swirl ratio and inlet loss coefficient as in the previous study and for the pre-swirl ratio and inlet loss coefficient obtained from the CFD analysis, respectively.

In the experiments, the OSI decreased with the development of the taper, while the FSI and eigenvalue analyses showed the opposite trend, with the OSI increasing with the taper. The following can be considered as possible causes: in the CFD analysis, the taper angle was assumed to be constant from the seal inlet to the seal outlet, but in reality the

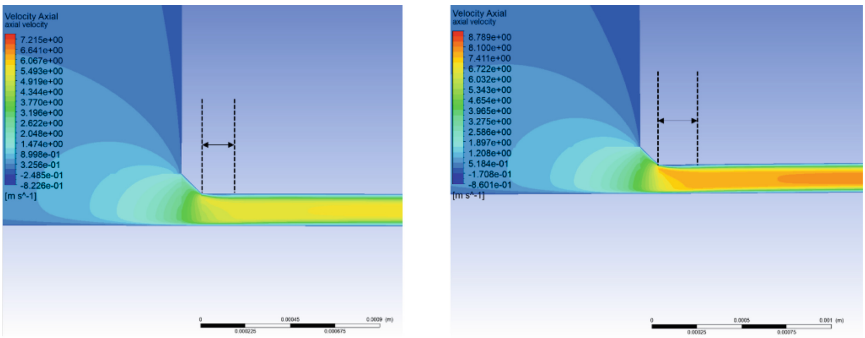

(a) Plain annular seal (b) Divergent tapered seal

Fig. 9. Contour of axial velocity for comparison of distance to reattachment

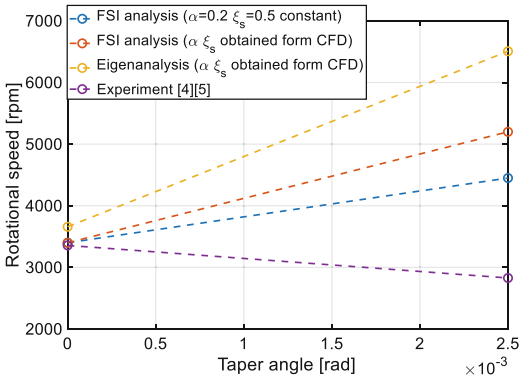

Fig. 10. Comparison of OSI obtained from FSI analysis, Eigenvalue analysis and experiment

magnitude of the taper angle varied depending on the axial position, as shown in Fig. 2. This may disturb the flow in the gap and cause a pressure loss. The pressure loss may have resulted in a weakening of the fluid film reaction force, which may have affected the OSI. In the FSI analysis, the pre-swirl ratio and loss coefficient were assumed to be constant in the circumferential direction, but in reality, the gap between the rotor and stator at the seal inlet is not constant due to rotor whirl, so these coefficients are not constant in the circumferential direction.

5 Conclusion

In this paper, the estimation of the pre-swirl and loss coefficients by CFD analysis is first presented. Furthermore, the FSI analysis for divergent tapered annular seal was extended from the conventional FSI analysis for the plain annular seal. The OSI obtained from the FSI analysis was compared with the OSI obtained from the experiments carried out in previous research and the following conclusions were drawn.

(1) The pre-swirl ratio increases with increasing rotational speed. The pre-swirl ratio for the plain annular seal is greater than that for the divergent tapered seal.
(2) The inlet loss coefficient of the plain annular seal increases with rotational speed, whereas the inlet loss coefficient of the divergent tapered annular seal is almost constant irrespective of the rotational speed.
(3) The FSI analysis of the divergent tapered annular taper seal with boundary condition parameters estimated by CFD analysis did not give the same OSI trend for the taper angle as in the experiment. It is necessary to conduct another experiment using a divergent tapered annular taper seal in the future.

References

1. Black, H.F.: Effects of hydraulic forces in annular pressure seals on the vibrations of centrifugal pump rotors. J. Mech. Eng. Sci. **11**(2), 206–213 (1969)
2. Nelson, C.C.: Analysis for leakage and rotor dynamic coefficients of surface roughened tapered annular gas seals. ASME J. Eng. Gas Turbines Power **106**(4), 927–934 (1984)
3. Ha, T.W., Choe, B.K.: Numerical simulation of rotordynamic coefficients for eccentric annular-type-plain-pump seal using CFD analysis. KSME J. Mech. Sci. Technol. **26**(8), 1043–1048 (2012)
4. Miyake, K., Inoue, T., Watanabe, Y.: Two-way coupling fluid–structure interaction analysis and tests of shaft vibration and clearance flow across plain annular seal. ASME J. Appl. Mech. **86**, 101002 (2019)
5. Kunori, Y., Inoue, T., Miyake, K.: Two-Way coupled shooting analysis of fluid force in the annular plain seal and vibration of the rotor system. ASME J. Vibr. Acoust. **143**, 051006 (2021)
6. Todd Lindsey, W., Childs, D.W.: The effects of converging and diverging axial taper on the rotordynamic coefficients of liquid annular pressure seals: theory versus experiment. ASME J. Vibr. Acoust. **122**, 126–131 (2000)
7. Yang, J., Andres, L.S.: On the influence of the entrance section on the rotordynamic performance of a pump seal with uniform clearance a sharp edge versus a round inlet. ASME J. Eng. Gas Turbines Power **141**, 031029 (2019)
8. ANSYS Fluent 2019 R3 User's Guide